Front. Phys. China, 2009, 4(1): 1–20
DOI 10.1007/s11467-009-0001-2

REVIEW ARTICLE

Hui ZHAI (翟荟)

Strongly interacting ultracold quantum gases

© Higher Education Press and Springer-Verlag 2009

Abstract This article reviews recent progresses in ultracold quantum gases, and it includes three subjects which are the Fermi gases across a Feshbach resonance, quantum gases in the optical lattices and the fast rotating quantum gases. In this article, we discuss many basic physics pictures and concepts in quantum gases, for examples, the resonant interaction, universality and condensation in the lowest Landau level; we introduce fundamental theoretical tools for studying these systems, such as mean-field theory for BEC-BCS crossover and for the boson Hubbard model; also, we emphasize the important unsolved problems in the forefront of this field, for instance, the temperature effect in optical lattices.

Keywords ultracold quantum gases, Feshbach resonance, optical lattice, rotating quantum gases

PACS numbers 67.85.-d, 67.85.Lm, 67.85.Hj, 67.85.Jk, 03.75.Ss

Contents

1 Introduction 1
2 Fermi gases across Feshbach resonance 2
2.1 Scattering resonance 2
2.2 Models for many-body systems 3
2.3 Universality 4
2.4 BEC-BCS crossover 5
2.5 Generalization of crossover physics 7
3 Quantum gases in optical lattices 9
3.1 Repulsive Bosons in lattices 10
3.2 Repulsive Fermions in Lattices 12
3.3 Lattice Fermi gases across a Feshbach resonance 14
4 Fast rotating quantum gases 16
4.1 Bosons in lowest Landau level 16
4.2 Fast rotating Fermi gases 17
5 Future prospects 18
Acknowledgements 18
References 18

Hui ZHAI (翟荟)[1, 2, 3, 4](✉)

[1] Center for Advanced Study, Tsinghua University, Beijing 100084, China
[2] Department of Physics, Ohio-State University, Columbus, OH 43210, USA
[3] Material Science Division, Lawrence Berkeley National Laboratory, Berkeley, CA 94720, USA
[4] Department of Physics, University of California at Berkeley, Berkeley, CA 94720, USA
E-mail: huizhai.physics@gmail.com

Received August 3, 2008; accepted August 24, 2008

1 Introduction

The realization of Bose-Einstein condensation in alkali atom gases in 1995 has opened up a new field of ultracold quantum gases. Roughly speaking, the development of this field has experienced three stages from then on. From 1995 to 2001, researches were mainly focused on the phenomena of Bose-Einstein condensates [1], which has enriched our knowledge of superfluidity a lot [2]. However, interactions are usually weak in these systems and most phenomena can be well understood based on a mean-field Gross-Pitaevskii equation. From 2002, the frontier of this field has moved to studying superfluidity in Fermi gases, after the degenerate Fermi gas was achieved and was found stable at a Feshbach resonance. As we will explain in Section 2, Fermi gas at resonance is a strongly interacting system. However, the strong interaction does not necessarily lead to a strongly correlated exotic state. Actually in the case of two-component Fermi gas with equal spin population, the ground state of the system remains superfluid despite the strong interactions. Even though, the ability of tuning interaction across a Feshbach resonance offers a wonderful opportunity to study the crossover from a Bose-Einstein

condensate to a Bardeen-Cooper-Schrieffer type superfluid. From 2002 to 2006, a lot of wonderful experiments and theoretical works have enabled us to understand the physics of BEC-BCS crossover with great depth [3−6], which will be briefly reviewed in Section 2. In 2007, this field has entered a new era. Many labs have begun to set up new experiments to study more strongly interacting systems in ultracold atomic gases, and the goal is to achieve strongly correlated new quantum states in a near future.

In some sense, it is actually relatively easier to achieve strong interactions in a gaseous system than in solids or liquids, because quantum gases are very dilute systems and the lower density means the smaller kinetic energy. For instance, the Fermi energy in an electron sample is usually several orders of magnitude larger than the interaction energy, while in a degenerate Fermi gas the Fermi energy can be easily tuned to be comparable to the interaction energy. So far, there are four major methods to achieve strong interactions in the cold atom systems. Besides using Feshbach resonance, the other three are imposing an optical lattice potential, rapidly rotating the system and reducing the dimensionality. In optical lattices, the motion of atoms becomes quantum hopping between different lattice sites and the hopping amplitude will be greatly reduced as the lattice barrier increases, which suppresses the kinetic energy so that the interaction energy becomes gradually dominative. An external rotating force is analogous to the magnetic gauge field, under which the single-particle spectrum becomes highly degenerated Landau levels. Within each Landau level the kinetic energy is completely quenched due to the degeneracy and therefore the physical properties of the system is entirely determined by the interactions. The progresses in these two aspects will be discussed in detail in Section 3 and 4 of this review. The strongly interacting effects in low-dimensional quantum gases will be discussed elsewhere.

2 Fermi gases across Feshbach resonance

2.1 Scattering resonance

The major character of quantum gases is its diluteness. Except in a few cases where magnetic or electronic dipole interactions are very strong, usually the interactions between atoms are dominated by short-range Van Der Waals interaction. For dilute gases with short-range interactions, the scattering problem can be treated by the partial wave expansion method, and in such an ultracold system, the s-wave scattering is the most dominative one compared to higher partial waves. Since the range of a Van Der Waals potential r_0 is much smaller than inter-particle spacing d, we only need to consider the asymptotic form of the scattering wave function

$$\psi = \frac{1}{kr}\sin(kr+\delta) \tag{1}$$

where r is the relative distance between two particles. Here the scattering phase shift δ is an important quantity. Since we are only interested in the low-energy scattering, we can expand δ to the lowest order of momentum k as $\delta = -ka_s$, where the expansion coefficient a_s is a quantity of length unit, which is called the s-wave scattering length. Hence, *in an ultra-cold dilute gas with short-range interactions, the interaction can be described by a single parameter, i.e. the s-wave scattering length* a_s. We note that this statement is valid even when a_s itself becomes very large near a scattering resonance. It is also useful to discuss a geometric meaning of a_s. For the zero-energy wave function $k \to 0$, by expanding the sin function to the lowest order of k, ψ becomes $1-a_s/r$, and $\psi = 0$ when $r = a_s$. In other words, a_s is the value of the node of the zero-energy wave function.

Here we use a simplified model potential to mimic the realistic Van Der Waals potential and to demonstrate the physical picture of a scattering resonance [7]. The model potential is displayed in Fig. 1. It diverges at $r = 0$ in order to mimic the hard-core repulsion of two atoms at very short distances, and therefore the wave function ψ has to vanish at $r = 0$. Between $r = 0$ and $r = r_0$, there is a short-range attractive part with the depth V_0. For $r > r_0$ the potential vanishes because the Van Der Waals potential is a short range potential. One can easily solve the zero-energy wave function for this potential. As shown in Fig. 1, for small V_0, a_s is a finite negative value. As V_0 increases, a_s becomes more and more negative and finally it reaches negative infinity at a critical value, and at the same value of V_0, a bound state appears at the threshold. With the further increase of

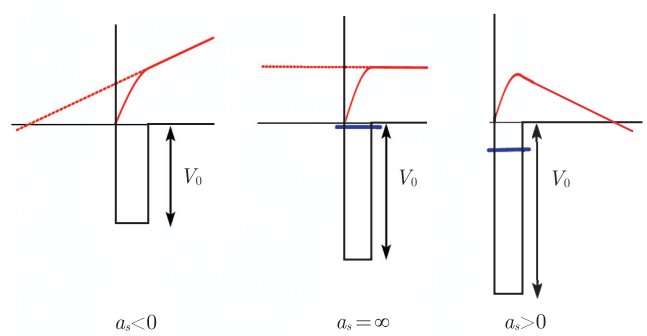

Fig. 1 Schematic of a model potential (*solid black line*), the zero-energy wave function (*solid red line*) and the bound state energy (*solid blue line*) for three different situations: $a_s < 0$, $a_s = \infty$ and $a_s > 0$.

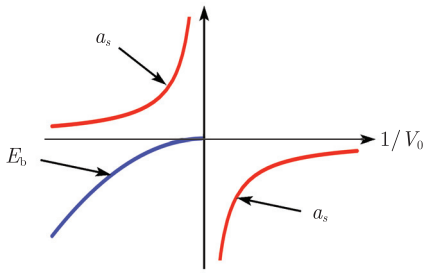

Fig. 2 Schematic of the scattering length (*red line*) and the bound state energy (*blue line*) as a function of $1/V_0$, where V_0 is the depth of the attractive part shown in Fig. 1.

V_0, a_s goes from positive infinity to finite positive value, and meanwhile the bound state energy becomes deeper and deeper. Hence, as shown in Fig. 2, on one side the resonance, a_s is negative, and the scattering states are stable. While on the other side of the resonance, a_s is positive, but the ground state of the two-atom system is actually not the scattering state but a two-body bound state.

Since in reality one cannot easily vary the shape of Van Der Waals potential, the way that a Feshbach resonance actually works is slightly more complicated. We first need to introduce the concept of "channels" in the scattering problem. Different "channels" have different total electronic spins of two atoms, and therefore have different Zeeman energy in the magnetic field. By changing the strength of the magnetic field, one can vary the Zeeman energy difference between different channels, and then tune the energy of a bound state in the "closed" channel to the threshold of the "open" channel. And because different channels are coupled through hyperfine interactions, the resonance with the bound state in the "closed" channel can also strongly affect the scattering length in the "open" channel.

Hence, the question arises as to what extent a two-channel scattering problem can be equivalently described by a single channel picture described above. To answer this question, the concepts of "broad resonance" and "narrow resonance" need to be introduced. A "broad resonance" means that the coupling strength between the "open" and the "closed" channels is much stronger compared to the typical kinetic energy of the scattered particles, which is the Fermi energy in a fermion gas. While a "narrow resonance" means the opposite. Here we will not go into the details of the discussion, but just present the conclusion, that is, for a "broad" Feshbach resonance, the physics can be well described by the single-channel picture [8]. Because all the Fermi gases experiments done so far are all about a "broad" resonance due to technical reasons, we will only focus on the "broad" resonance in this article.

2.2 Models for many-body systems

We now come to the discussion of the many-body Hamiltonian for dilute gases. In summary, there are three widely used Hamiltonians and all of three are equivalent in the "broad" resonance limit.

The first one is zero-range "pseudo-potential" introduced by Huang and Yang [9]. Since in general a many-body system is easier to deal with if the interactions are all local, i.e. zero-ranged, and also as we have discussed above, since a_s is the only important quality in the low-energy scattering, the question is whether one can find out a zero-range potential which produces the same a_s as real Van Der Waals potential. If such a zero-range potential does exit, we can replace real Van Der Waals potential with a short-range contact interaction. Actually, such a "pseudo potential" was first found in Ref. [9], which can be written as

$$V_s(\boldsymbol{r}_1-\boldsymbol{r}_2)=\frac{4\pi\hbar^2 a_s}{m}\delta(\boldsymbol{r}_1-\boldsymbol{r}_2)\partial_{\boldsymbol{r}_1-\boldsymbol{r}_2}(\boldsymbol{r}_1-\boldsymbol{r}_2) \quad (2)$$

Thus, the many-body Hamiltonian is simply $\boldsymbol{H}=\sum_i H_0(\boldsymbol{r}_i)+\sum_{ij}V_s(\boldsymbol{r}_1-\boldsymbol{r}_2)$, where H_0 is the single body Hamiltonian. The advantage of this Hamiltonian is that the short-range divergency cut off has been explicitly implemented by the partial derivative in the "pseudo-potential", while the disadvantage is also due to the partial derivative, the calculation becomes more complicated and subtle.

The second one is δ-function potential. If one ignores the partial derivative in the pseudo-potential of Eq. (2), the interaction simply becomes $V_g=g\delta(\boldsymbol{r}_1-\boldsymbol{r}_2)$. The calculation therefore becomes much simpler, but the price to pay is that one will encounter short-range divergency everywhere in the calculation. The reason is that the δ function potential is ill-defined, and the coupling constant "g" is not a physical parameter. To relate "g" with the physical parameter of the scattering length a_s, one should use V_g to calculate a T-matrix of a two-body problem, which gives

$$\begin{aligned}\frac{4\pi\hbar^2 a_s}{m}&=T=g+g\sum_{\boldsymbol{k}}\frac{1}{\hbar^2k^2/m}g+\cdots\\&=\frac{g}{1-g\sum_{\boldsymbol{k}}m/(\hbar^2k^2)}\end{aligned} \quad (3)$$

and therefore

$$\frac{1}{g}=\frac{m}{4\pi\hbar^2 a_s}-\sum_{\boldsymbol{k}}\frac{m}{\hbar^2k^2} \quad (4)$$

Using V_g, the many-body Hamiltonian for the spin-1/2 Fermi gases can be written as

$$\boldsymbol{H} = \sum_{\sigma=\uparrow,\downarrow} \int \mathrm{d}^3\boldsymbol{r}\psi_\sigma^\dagger(\boldsymbol{r})\hat{H}_0\psi_\sigma(\boldsymbol{r}) + g\int \mathrm{d}^3\boldsymbol{r}\psi_\uparrow^\dagger(\boldsymbol{r})\psi_\downarrow^\dagger(\boldsymbol{r})\psi_\downarrow(\boldsymbol{r})\psi_\uparrow(\boldsymbol{r}) \quad (5)$$

But we should always keep in mind that in the calculation, we always need to use Eq. (4) to relate "g" to a_s, and the second term in the r.h.s of Eq. (4) will automatically eliminate the short wave length divergency.

The above two models belong to the so-called "single-channel" description. The third model introduced here is based on the sprit of two-channel picture. We first introduce a bosonic field of $\boldsymbol{b}(\boldsymbol{r})$ for the close channel molecules, and the scattering processes are described by a conversion term between open channel fermion fields and the molecular $\boldsymbol{b}(\boldsymbol{r})$ field. Again, using spin-1/2 Fermi gases as an example, the many-body Hamiltonian should be written as

$$\begin{aligned}\boldsymbol{H} = &\sum_{\sigma=\uparrow,\downarrow} \int \mathrm{d}^3\boldsymbol{r}\psi_\sigma^\dagger(\boldsymbol{r})\hat{H}_0\psi_\sigma(\boldsymbol{r}) \\ &+ \int \mathrm{d}^3\boldsymbol{r} b^\dagger(\boldsymbol{r})\hat{H}_0^b b(\boldsymbol{r}) + \nu b^\dagger(\boldsymbol{r})b(\boldsymbol{r}) \\ &+\alpha\int \mathrm{d}^3\boldsymbol{r}\psi_\uparrow^\dagger(\boldsymbol{r})\psi_\downarrow^\dagger(\boldsymbol{r})b(\boldsymbol{r}) \\ &+\alpha^*\int \mathrm{d}^3\boldsymbol{r} b^\dagger(\boldsymbol{r})\psi_\downarrow(\boldsymbol{r})\psi_\uparrow(\boldsymbol{r})\end{aligned} \quad (6)$$

where the molecular detuning ν and the conversion strength α are two "model" parameters.

To relate these two model parameters with real physical parameters, we again try to solve a two-body problem with Hamiltonian Eq. (6) in free space. The wave function can be generally written as $|\Psi\rangle = (\beta\boldsymbol{b}^\dagger + \sum_{\boldsymbol{k}}\eta_{\boldsymbol{k}}\psi_{\boldsymbol{k}\uparrow}^\dagger\psi_{-\boldsymbol{k}\downarrow}^\dagger)|0\rangle$. Thus, the eigenequation $\boldsymbol{H}|\Psi\rangle = E|\Psi\rangle$ will lead to two coupled equations, that is, $\nu\beta + \alpha\sum_{\boldsymbol{k}}\eta_{\boldsymbol{k}}/\sqrt{L^3} = E\beta$, and $\hbar^2k^2\eta_{\boldsymbol{k}}/m + \alpha^*\beta/\sqrt{L^3} = E\eta_{\boldsymbol{k}}$, where L is the length of the system. These coupled equations lead to a self-consistent equation for eigenenergy

$$\begin{aligned}\nu - E &= \frac{|\alpha|^2}{L^3}\sum_{\boldsymbol{k}}\frac{1}{\hbar^2k^2/m - E} \\ &= \frac{|\alpha|^2}{2\pi^2}\int \mathrm{d}k k^2 \frac{1}{\hbar^2k^2/m - E}\end{aligned} \quad (7)$$

The r.h.s. of Eq. (7) of this integral has short wave length divergency, which can be eliminated by renormalizing

$$\nu_0 = \nu - \frac{|\alpha|^2}{2\pi^2}\int \mathrm{d}k k^2 \frac{1}{\hbar^2k^2/m} \quad (8)$$

and Eq. (7) becomes

$$\nu_0 - E = \frac{|\alpha|^2}{2\pi^2}\int \mathrm{d}k k^2\left(\frac{1}{\hbar^2k^2/m - E} - \frac{1}{\hbar^2k^2/m}\right) \quad (9)$$

For the bound state with $E < 0$, we have $\nu_0 - E = -|\alpha|^2 m^{3/2}\sqrt{-E}/(4\pi^2\hbar^3)$, and this is the equation for the bound state energy obtained from the model of Eq. (6). On the other hand, we have the well-known results for the bound state energy from quantum mechanical scattering theory, that is, $\sqrt{-E} = \hbar/(a_s\sqrt{m}) - r_0\sqrt{m}E/(2\hbar)$, where r_0 is the effective range of the scattering potential. Comparing these two equations, we can establish the relation between ν, α and the physical parameters r_0 and a_s

$$\frac{1}{\alpha^2} = -\frac{r_0 m^2}{8\pi^2\hbar^4} \quad \text{and} \quad \frac{\nu_0}{\alpha^2} = -\frac{m}{a_s 4\pi^2\hbar^2} \quad (10)$$

The so-called "broad" resonance in a Fermi system means $k_\mathrm{F}r_0 \ll 1$, that is to say, the conversion coupling α is much larger than the Fermi energy. In other words, this means the bound state involved in resonance will couple to all open channel fermions from the bottom to the top of the Fermi sea with almost identical strength. Hence, one can image that the weight of the wave function on the close-channel bound state will be heavily depleted by the open channels states and become very small, and the properties of the many-body system will be dominated by the fermions in the scattering states. This provides us an intuition why in a "broad" resonance the close-channel molecules are not important and the two-channel description is equivalent to the single-channel model.

There are other models like "model potential" [12] and "separable potential" [23] which are less popularly used, and we will not discuss them here.

2.3 Universality

The theory for dilute gases was first developed in the 1950s by Lee, Huang and Yang [9−11]. They considered the regime where the gas parameter $na_s^3 < 1$ and therefore one can treat the interaction perturbatively. In this regime, the physical quantities, such as the ground state energy, can be expressed in terms of $k_\mathrm{F}a_s$ as [11]

$$\frac{E}{N} = \frac{3}{5}E_\mathrm{F}\left[1 + \frac{10}{9\pi}k_\mathrm{F}a_s + \frac{4(11-2\lg 2)}{21\pi^2}(k_\mathrm{F}a_s)^2 + \cdots\right] \quad (11)$$

However, such a theory will fail when the gas parameter $na_s^3 > 1$. Here we will introduce the concept of "universality" in a many body fermionic system at unitarity, where the scattering length a_s greatly exceeds the inter-particle spacing and even diverges, while the range

of the scattering potential r_0 is negligible for a "broad" resonance. For infinite a_s, it is obvious that any physical quantity cannot depend on $(k_{\rm F}a_s)^n$ with positive n and also $(k_{\rm F}a_s)^n = 0$ for any negative n. From this simple argument one can conjecture that any physical quantity will not depend on a_s at unitarity [13]. Remember in the previous section we have shown that a_s is the only relevant parameter for the low energy scattering for a broad resonance, the physical quantity therefore depends on *only one* length scale, which is the inter-particle spacing d. A typical example is that the ground state energy at unitarity will be

$$\frac{E}{N} = (1+\beta)\frac{3}{5}E_{\rm F} \tag{12}$$

where β is a universal number and the Monte-Carlo calculation predicts $\beta = -0.58 \pm 0.01$ [14, 15]. Recent experiments in both ^{6}Li and ^{40}K gas have confirmed this number within experimental accuracy [16, 17]. Note that the details of inter-atomic potential are very different for lithium and potassium, the fact that the number β is independent of atomic species provides strong experimental evidence of "universality".

At finite temperature, the statement of "universality" is that any physical quantity $\mathcal{G}$ is a function of density n and $T/T_{\rm F}$ only. For instance, from dimension analysis, the energy can be expressed as

$$E = NE_{\rm F} f\left(\frac{T}{T_{\rm F}}\right) \tag{13}$$

and the entropy is

$$S = Nk_{\rm B} g\left(\frac{T}{T_{\rm F}}\right) \tag{14}$$

Note that the local pressure is determined by $-\partial E/\partial V$ with fixed particle number N and entropy S, and Eq. (14) shows that fixing entropy is equivalent to fixing temperature. Hence, we reach a useful expression that pressure is proportional to local energy volume density $\mathcal{E}$ [13, 18]

$$P = \frac{2}{3}\frac{E}{V} = \frac{2}{3}\mathcal{E}\left(n, \frac{T}{T_{\rm F}}\right) \tag{15}$$

This is a very useful relation, and surprisingly, it works for both a strongly interacting resonant gas and a non-interacting gas.

For a trapped gas, the mechanical equilibrium and force balance yields

$$\nabla P(\boldsymbol{r}) + n(\boldsymbol{r})\nabla U(\boldsymbol{r}) = 0 \tag{16}$$

where $U(\boldsymbol{r})$ is the trapping potential. Note that $\boldsymbol{r}\nabla U(\boldsymbol{r}) = 2U(\boldsymbol{r})$ for the hamonic trap, after integrating over $\mathrm{d}^3\boldsymbol{r}$ and performing integration by part for $\boldsymbol{r}\nabla P(\boldsymbol{r})$, it yields

$$N\langle U(\boldsymbol{r})\rangle = \frac{3}{2}\int \mathrm{d}^3\boldsymbol{r} P(\boldsymbol{r}) = \frac{E}{2} \tag{17}$$

The l.h.s. of Eq. (17) is a measurable quantity in experiment, through which one can measure the energy of a strongly interacting gas.

An intriguing problem is how to determine temperature for a strongly interacting system. In a weakly interacting BEC or a degenerate Fermi gas, temperature is determined by fitting density profile using a known equation-of-state. However, since the equation-of-state is not known for the strongly interacting system, the question is whether there is a *model-independent* way to measure temperature. The thermodynamic relations discussed above will help us to establish a model-independent measurement of temperature. Since entropy can be measured by adiabatically swapping the magnetic field to tune the scattering length to a weakly interacting regime, the entropy can be determined by using the known equation-of-state. On the other hand, energy can be measured by the method discussed above. Hence, $\partial S/\partial E = 1/T$ gives a model-independent measurement of temperature [19]. This method has now become standard in later studies of strongly interacting Fermi gases.

2.4 BEC-BCS crossover

In the above, we discussed the thermodynamic properties in the resonance regime. Now we will discuss the ground state at resonance. In general, the ground state is hard to describe in a non-perturbative regime. However, in this situation it is very lucky. Since we know that in one limit where $1/(k_{\rm F}a_s) \ll 0$, the system is a weakly attractive Fermi gas, and the ground state is a BCS state; while in the other limit where $1/(k_{\rm F}a_s) \gg 0$, each pair of fermions will form two-body bound state of bosonic molecules, and from the four-body calculation we know that the interaction between molecules is $a_{\rm m} = 0.6a_s$ [15, 20], which is repulsive in this regime, thus the ground state is a Bose condensate of those molecules. Leggett noticed that both BCS and BEC have the same symmetry and they can both be described by a BCS-like wave function [21, 22]:

$$|\Psi\rangle = \prod_{\boldsymbol{k}}\left(u_{\boldsymbol{k}} + v_{\boldsymbol{k}} c^\dagger_{\boldsymbol{k}\uparrow} c^\dagger_{-k\downarrow}\right)|0\rangle \tag{18}$$

Based on this observation, one can conjecture that it is a *crossover* that connects the BCS regime to the BEC regime, and throughout the crossover, the ground state can be approximately described by a wave function like

Eq. (18). In other words, the ground state at resonance is adiabatically connected to these two weakly interacting regimes.

The physical picture of this crossover is shown in Fig. 3. In the BEC regime, the inter-particle spacing d is much smaller than the size of a fermion pair ξ, and therefore one can view those pairs as bosons. In contrast, the inter-particle spacing d is much larger than the size of fermion pairs ξ in the BCS regime. In between, as the attraction increases, the size of Cooper pairs continuously shrinks, and in the unitary regime, the size of Cooper pairs and the inter-particle spacing are comparable. In particular, exactly at resonance, $\xi = \alpha d$ where α is a universal constant, which gives a microscopic view of "universality".

This physics can be quantitatively described by a mean-field theory using Eq. (18) as a trial wavefunction [21, 22]. The standard BCS type mean-field theory will give rise to two equations. The first equation is the gap equation,

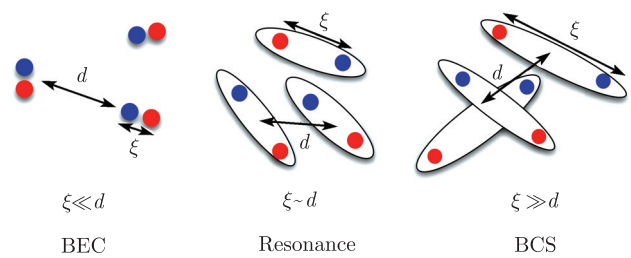

Fig. 3 A schematic illustration of the crossover from the BEC to the BCS regime, d is the average inter-particle spacing and ξ is the Cooper pair size.

$$\frac{m}{4\pi\hbar^2 a_s} = \sum_{\boldsymbol{k}} \left(\frac{1}{2\sqrt{\left(\frac{\hbar^2 k^2}{2m} - \mu\right)^2 + \Delta^2}} - \frac{1}{\frac{\hbar^2 k^2}{m}} \right) \tag{19}$$

where $\Delta = \sum_{\boldsymbol{k}} u_{\boldsymbol{k}} v_{\boldsymbol{k}}$, and the second equation is the number equation

$$N = \sum_{\boldsymbol{k}} \frac{1}{2} \left[1 - \frac{\frac{\hbar^2 k^2}{2m} - \mu}{\sqrt{\left(\frac{\hbar^2 k^2}{2m} - \mu\right)^2 + \Delta^2}} \right] \tag{20}$$

which determines how chemical potential changes as the interaction varies. The solution of these two coupled equations is displayed in Fig. 4. Fig. 4(a) shows that the pairing gap monotonically increases as it approaches the BEC side, and it eventually approaches $\sqrt{3}E_{\rm b}/2$, where $E_{\rm b}$ is the binding energy of molecules. Figure 4(b) shows how the chemical potential is renormalized from BCS to BEC. In the weakly interacting BCS side, the chemical potential is about free fermion Fermi energy. As the attraction increases, the chemical potential keeps decreasing, eventually at the BEC side it approaches $-E_{\rm b}/2$, and the excitation energy for pair breaking is therefore $\sqrt{\mu^2 + \Delta^2} = -E_{\rm b}$. We emphasize that the strong interaction dependence of the chemical potential is a major feature of BEC-BCS crossover.

Though there is no phase transition between BEC and BCS, they still have significant difference especially in terms of the low energy excitations, as shown in Fig. 5. In the BCS regime where $\mu > 0$, the fermionic excitation has a small gap of Δ, while the velocity of the bosonic Goldstone mode is proportional to the Fermi velocity, which is relatively large. So the low energy excitations are dominated by pair breaking. In the BEC regime where $\mu < 0$, the fermionic excitation of pair breaking has a gap of $\sqrt{\Delta^2 + \mu^2}$, which becomes very large, while the velocity of the bosonic mode becomes $\sim \sqrt{\pi a_{\rm m} n}/m$ which is very soft. So in this regime, the low energy excitations are dominated by Bogoliubov mode of finite momentum fermion pairs. However, we emphasize that this Bogoliubov mode is not captured by the mean-field theory discussed above, which makes this theory less accurate in the BEC side than in the BCS side. A better description of the BEC side $[-1/(k_{\rm F} a_s) < -1]$ will be a Bogoliubov type mean-field theory of bosonic molecules

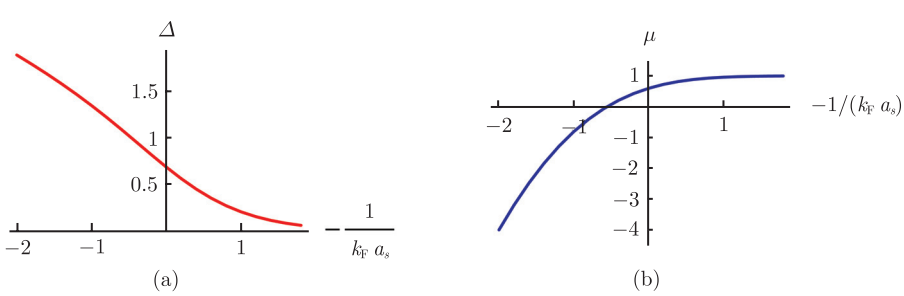

Fig. 4 **(a)** The pairing gap Δ as a function of $-1/(k_{\rm F} a_s)$ and **(b)** the chemical potential μ as a function of $-1/(k_{\rm F} a_s)$.

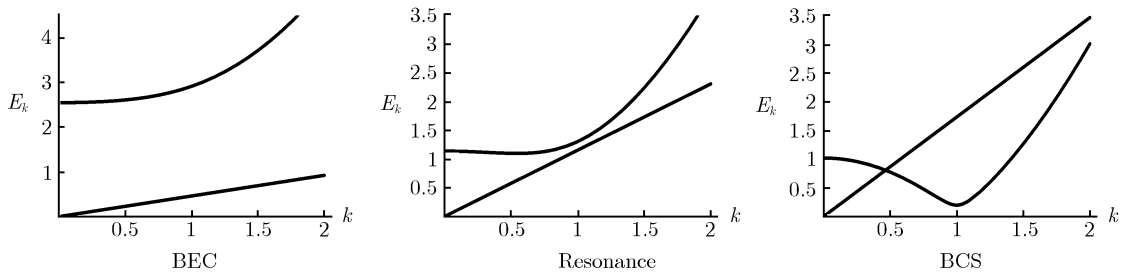

Fig. 5 Schematic of the low-energy excitation spectrum for both fermionic and bosonic modes in the BEC, the unitary and the BCS regime.

which incorporates finite momentum quantum depletion of the condensate. And in the unitary regime, both of these two excitation modes are equally important. A theory that can capture both two modes are highly desirable, especially for describing finite temperature properties.

We close this subsection by presenting a classification of Fermi gases around a scattering resonance, as shown in Fig. 6. As discussed above, across a Feshbach resonance, the system undergoes a crossover from a weakly interacting BCS state to a resonant superfluid and eventually to a condensate of bosonic molecules. Besides, in the regime with positive scattering length, fermions in the scattering states experience repulsive interactions, and they are meta-stable if the bound state is sufficiently deep.

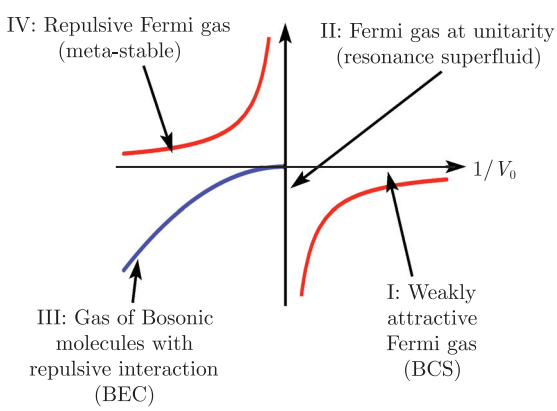

Fig. 6 A schematic of the scattering length and the bound state energy in a two-body problem (the same as Fig. 2), and the classification of many-body Fermi gases in various regimes.

2.5 Generalization of crossover physics

In the above two subsections, we have discussed that, on one hand, at resonance the interactions are so strong that the total interaction energy is comparable to kinetic energy, and its effects is non-perturbative. On the other hand, we have introduced the crossover scenario in which the ground state at resonance remains pretty much a weakly correlated superfluid. We emphasize that the reason is because the strongly interacting regime can be adiabatically connected to two weakly interacting limits by tuning some physical parameters, and the quantum state in these two limits can be adiabatically deformed into each other. Therefore, a natural idea to reveal stronger correlation at resonance is to destroy superfluidity, and subsequently destroy the adiabatic connection between the quantum state at resonance and those in two weakly interacting limits.

The most natural way to destroy superfluidity is through increasing temperature. In the BCS side, increasing temperature will lead to Cooper pair breaking which destroys superfluid, and the revealed normal state is a normal Fermi liquid. The critical temperature increases as attraction increases; while in the BEC side, the superfluid transition is the condensation of the molecules, above which the phase coherence between molecules is lost and it becomes a bosonic normal state, and the critical temperature is almost constant once the density is fixed. It is very clear that the normal states in two sides are very different. Therefore, the normal state at resonance becomes very intriguing since there presents both the Cooper pair breaking effects and the incoherent Cooper pairs. A theory on superfluid critical temperature was first proposed by Noziéres and Schmitt-Rink [23].

Nevertheless, we are more interested in revealing more interesting normal states at zero or very low temperatures. There are various ways to frustrate superfluidity, and each of them will lead to rich physics. Here we list a few examples:

(1) An optical lattice potential can destroy the superfluid by driving a transition from the superfluid state to an insulator, and different insulating states will be reached in different sides of the resonance. In the BEC side it will be a Mott insulator of bosonic molecules, and in the BCS side it will be a band insulator fermionic atoms. A general picture of superfluid to insulator transition throughout the crossover regime will be discussed in Section 3.3 in detail.

(2) Rotating a superfluid can mimic applying a magnetic field to superconductor. At some critical strength of rotation, superfluid will be destroyed. At the extreme fast rotation limit, fermionic and bosonic quantum Hall states will be reached in the BCS side and in the BEC side, respectively. In Section 4.2 we will discuss how the BEC-BCS superfluid family responds to an external rotation and how the crossover scenario breaks down in the extreme fast rotation limit.

(3) In cold atom experiments, it is very easy to create the situation that the population of two spin components are unequal [17, 24, 25]. This mimics a Zeeman field in electron systems, and in this system, the effective Zeeman field can be as large as comparable to the Fermi energy. In a BCS superfluid, it is known as the Pauli limit that a Zeeman field will drive a first order transition to normal state when the Zeeman energy is comparable to the pairing gap. While in the BEC side, note that the two-body bound state is stable in vacuum, the minority fermions can always find their partner in the majority component to form a molecular state, and these molecules can always Bose condense even if they are very dilute in large imbalance limit. So the system remains superfluid mixed with residual majority fermions. As schematically shown in Fig. 7, it is clear that these two sides respond differently to the Zeeman field, and it stimulates a lot of research on how the transition between these two regimes takes place [26]. The interesting question is at the strongly interacting resonance regime, whether there is still a Pauli limit of superfluidity. If there is, whether the normal state at large population imbalance is still a Fermi liquid, and if it is, it must be a Fermi liquid with universal properties which is of great interest.

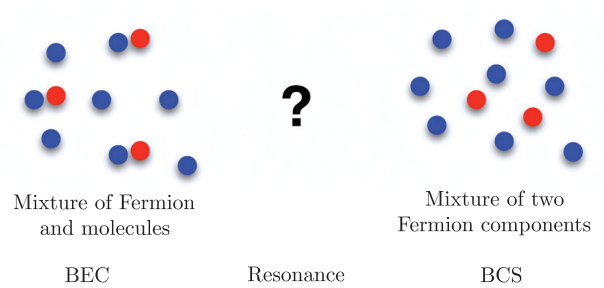

Fig. 7 Schematic of quantum states at large population imbalance at the BEC side and the BCS side.

In addition to these, there are other two generalizations of crossover physics which are very interesting, and they are being studied by ongoing experiments.

(4) In a mixture of two different fermion species, like mixture of ^{40}K and ^{6}Li, two "spin components" have different masses. Recently, Feshbach resonance between different atomic species has been found [27], which opens a new route to study crossover physics with unequal masses mixture. Note that for equal population, though the Fermi energies of two components are quite different due to mass difference, it still possesses Cooper instability since they have the same size of the Fermi surfaces. This BCS superfluid will undergo a crossover to a BEC of heteronuclear molecules. Although from this point of view, the ground state properties of unequal masses mixture is very similar to the equal mass one, the excitation spectrum strongly depends on the mass imbalance, which leads to more interesting finite temperature properties and a lot more intriguing physics when Zeeman field, rotation or optical lattice is imposed.

(5) Alkali atoms usually have more than two hyperfine spin states. Take ^{6}Li as an example, in the magnetic field there are three states in the lower hyperfine branch, and all of them can be easily trapped. Previously, two out of three states have been used to study crossover physics in experiments, which possesses resonance at about 830 G. Actually, the third state also has Feshbach resonances with these two in the regime nearby 800 G, as shown in Fig. 8 [28]. Multi-component mixture of fermions is a very interesting subject, especially when the interaction between them are all very strong and highly tunable [29]. For example, the phase diagram of a three-component mixture with a density ratio of 1 : 2 : 1 has been studied in Ref. [30] and shown in Fig. 8. In the BEC side of two resonances, two kinds of molecules are stable and the ground state is a binary mixture of a two-component molecular condensate, while superfluidity will break down due to the mismatch of three Fermi surfaces as it approaches the BCS side, which is similar to the physics discussed in the content of imbalance mixture of two-component fermions. The physics of multi-component mixture will also strongly depend on

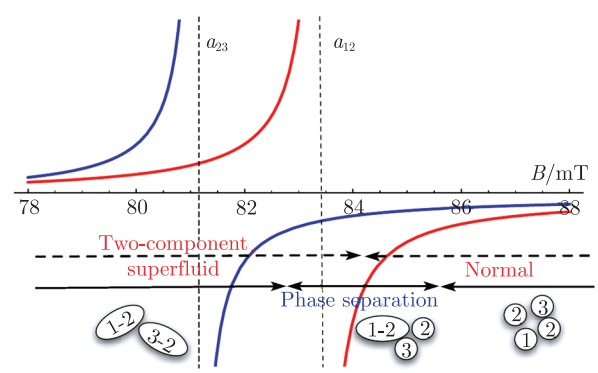

Fig. 8 Schematic of phase diagram as a function of magnetic field which controls the scattering length, in a mixture of lowest three hyperfine spin states of ^{6}Li gases. This phase diagram was initially published in Ref. [30].

the concentration ratio of different components and the regime of the magnetic field which controls the relative strengths and sign of the scattering lengths. Recently, some preliminary experimental work on the stability of three-component mixtures has been reported [31], which will stimulate more work on this subject.

3 Quantum gases in optical lattices

When a laser field forms a standing wave along the x direction in space, atoms will experience a periodic potential in the form of $V_0 \sin^2(Kx)$ due to the AC Stark effect, where $K = \pi/\lambda$ and λ is the wave length of the laser. When three independent laser fields are turned on along three spatial directions, it will form a three-dimensional lattice potential as $V_x \sin^2(Kx) + V_y \sin^2(Ky) + V_z \sin^2(Kz)$. This kind of period potential is referred to as optical lattices, which has now become a major tool and playground for studying many-body problems in ultra-cold quantum gases. By tuning the intensity of the laser field, one can independently control V_x, V_y and V_z, so that the system can go from a tunneling dominated regime to interaction dominated regime continuously. Moreover, optical lattices provide accessibility to low-dimensional physics. If one tunes $V_x \sim V_y \gg V_z$, the system becomes arrays of almost independent one-dimensional tubes; and if one tunes $V_z \gg V_x \sim V_y$, the system behaves like layers of independent two-dimensional pancakes.

As we know from text books on solid state physics, single-particle spectrum in a periodic potential exhibits band structure. For instance, the single-particle density of state in a three-dimensional cubic lattices is shown in Fig. 9(a). For very shallow lattices, the density-of-state is finite everywhere as indicated by the dashed line in Fig. 9(a). However, when V_0 is above a certain critical value, a band gap opens where the single-particle density-of-state vanishes, as indicated by the solid line in Fig. 9(a). The band gap increases rather quickly with the increase of lattice depth V_0, as shown in Fig. 9(b).

As for the interactions in optical lattices, here are a few general comments. (1) Except in a few exceptions, like chromium atoms or heteronuclear molecules where the dipolar interaction is profound, usually the interaction between atoms are short ranged and therefore only the on-site interaction needs to be considered in optical lattices. (2) Unless close to a Feshbach resonance, usually the s-wave scattering length $a_{\rm s}$ is a few nano-meters, while the lattice constant $\lambda = \pi/K \sim$ μm, and the harmonic length of each lattice size is at least two orders of magnitudes larger than a_s, hence the s-wave approximation will still be applicable in optical lattices. (3) When the interaction is away from a resonance, the interaction energy can be estimated as

$$U \sim \frac{4\pi\hbar^2 a_s}{m\lambda^3} \sim \frac{a_s}{\lambda} E_{\rm R} \ll E_{\rm R} \tag{21}$$

In the discussion of optical lattices, we usually use so-called "photon recoil energy" $E_{\rm R} = \hbar^2 K^2/(2m)$ as the energy unit. Hence, for bosons in optical lattices, when V_0 is above $(3-4)E_{\rm R}$, the band gap is larger than $1E_{\rm R}$ as shown in Fig. 9(b), and one can safely use single-band boson Hubbard model to describe the physics. The basic physics content and experimental progresses on boson Hubbard model will be discussed in Section 3.1. While for two-component fermions, if the filling number is smaller than two, the physics can also be described as single s-band model, which gives the famous fermion Hubbard model. Nowadays, many labs are pursuing experiments where one can use cold Fermi gases to simulate the fermion Hubbard model to shed light on many long-standing condensed matter problems, including High-$T_{\rm c}$ problem. We will discuss this and its related issues in Section 3.2. However, when the interaction is close to a resonance, a_s becomes comparable or even larger than λ, which means the interaction energy will be strong enough to compete with the band gap. In this situation,

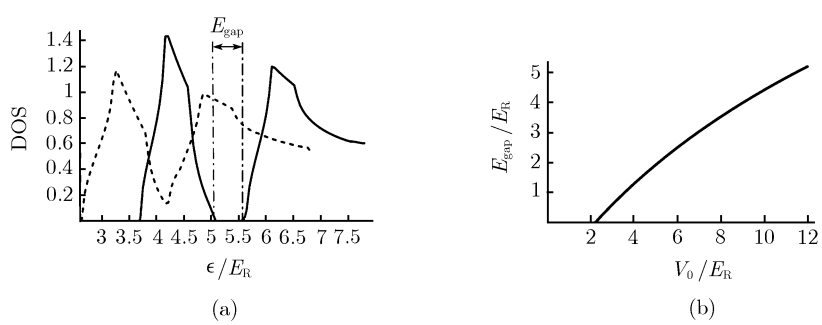

Fig. 9 **(a)** Single-particle density of state for a three-dimensional lattice with $V_x = V_y = V_z = V_0 = 2E_{\rm R}$ (*dashed line*) and $V_0 = 3E_{\rm R}$ (*solid line*) respectively. **(b)** The band gap between s-band and p-band, as a function of V_0.

the single-band model will be no longer applicable and one needs more complicated multi-band model to capture the essential physics of lattice gases with resonance interaction, where a host of new quantum many-body physics remains to be explored. We will talk about this in Section 3.3.

3.1 Repulsive Bosons in lattices

The single band boson Hubbard model is written as follows

$$\hat{H} = -t\sum_{ij}\hat{b}_i^\dagger\hat{b}_j + \sum_i\left[\frac{U}{2}\hat{n}_i(\hat{n}_i-1) - \mu\hat{n}_i\right] \tag{22}$$

where $t = \int \mathrm{d}^3\boldsymbol{r}w^*(\boldsymbol{r}-\boldsymbol{R}_i)V(\boldsymbol{r})w(\boldsymbol{r}-\boldsymbol{R}_j)$ is the tunneling amplitude. $w(\boldsymbol{r}-\boldsymbol{R}_i)$ is the wannier wave function localized at i-site. $U = 8\pi\hbar a_\mathrm{s}/m\int \mathrm{d}^3\boldsymbol{r}|w(\boldsymbol{r}-\boldsymbol{R}_i)|^4$ which describes the strength of on-site interaction, μ is the chemical potential, and $\hat{n}_i = \hat{b}_i^\dagger\hat{b}_i$ is the boson number operator at site-i.

It is easy to show that there are two distinct phases in this model. In the limit of $t = 0$, the ground state is an eigenstate of each $\hat{n}_i$ which is of the form $|\psi\rangle = \prod_i \hat{b}_i^{\dagger n_i}|0\rangle$. The excitation in this limit is either adding a particle in one site or taking a particle away from one site, which will cause a finite excitation energy on the order of U. This state is called a Mott insulator. On the opposite limit of non-interacting bosons with $U = 0$, the ground state is a Bose-Einstein condensate at zero-momentum state, and $|\psi\rangle = \left(\sum_i \hat{b}_i^\dagger\right)^N/\sqrt{N!}|0\rangle$. It possesses the off-diagonal long range order and gapless excitation. Hence, as a function of t/U, there must be a quantum phase transition that separates these two phases [32].

The phase diagram and the phase transition can be described by a simple mean field theory [33]. We decompose the kinetic term into

$$-t\sum_{ij}\hat{b}_i^\dagger\hat{b}_j = \sum_i\left(-\varphi\hat{b}_i^\dagger - \varphi^*\hat{b}_i + \frac{|\varphi|^2}{zt}\right) \tag{23}$$

where $\varphi = zt\langle\hat{b}_i\rangle$ is the superfluid order parameter, and z is the number of adjacent sites of site-i. In this mean-field we only consider the uniform quantum states, and the entire Hamiltonian becomes a sum of each lattice site as $\boldsymbol{H} = \sum_i \boldsymbol{H}_i$ where

$$\boldsymbol{H}_i = -\varphi\hat{b}_i^\dagger - \varphi^*\hat{b}_i + \frac{|\varphi|^2}{zt} + \frac{U}{2}\hat{n}_i(\hat{n}_i-1) - \mu\hat{n}_i \tag{24}$$

The ground state energy of $\boldsymbol{H}_i$, $F(\varphi)$, can be easily calculated. Then one can minimize $F(\varphi)$ with respect to φ, and it will yield either zero or non-zero φ, which corresponds to a Mott insulator or a superfluid, respectively. Two typical situations are displayed in Fig. 10(a). For small t/U, the minimum occurs at $\varphi = 0$. As the increase of t/U, the minimum departures from zero to a non-zero φ, which marks the insulator to superfluid transition.

With this mean-field scheme, one can obtain the phase diagram of the boson Hubbard model as shown in Fig. 10(b). In the regime of small t/U, there are lobs of Mott insulators, and the Mott lobs shrink with the increase of the chemical potential and the boson filling number. This is an effect due to the boson enhancement factor, that is, the number fluctuation on top of a Mott insulator with n particle per site will get an enhancement factor of $\sqrt{n}$. Hence, the Mott insulator with larger filling number is easier to become a superfluid.

This phase diagram of Fig. 10(b) is for a homogeneous system. For the cold atom experiments which are usually performed in a harmonic trap, one has to use local density approximation (LDA) to relate this phase diagram to the real space density profile. The idea of LDA is to treat the system locally as a bulk system with a chemical potential $\mu_0 - V(\boldsymbol{r})$, where μ_0 is the chemical potential at the center of the cloud and $V(\boldsymbol{r})$ is the trapping potential. Hence, from the center to the edge, the chemical potential trajectory $\mu(\boldsymbol{r})$ goes from μ_0 to zero, as indicated by the dashed line in Fig. 10(b) and the inset of Fig. 11(a). Depending on which phase $\mu(\mathbf{r})$ lies in, the system locally behaves as either a superfluid or a Mott insulator. If $\mu(\boldsymbol{r})$ is in the superfluid phase, the density is a smooth function that continuously changes as a function of the position $\boldsymbol{r}$, while if $\mu(\boldsymbol{r})$ is in the Mott insulator phase, the density will exhibit a plateau due to the incommensurate nature of the insulator. The whole cloud therefore exhibits shell structure of separated phases, which is usually referred to the wedding cake structure, as shown in Fig. 11(a).

The first experimental signature of the phase transition was reported in Ref. [34], which stimulated a lot of theoretical and experimental works in recent years [35]. In experiments, the Mott insulator is relatively easy to identify. For example, from the transport experiment [34] or radio-frequency spectroscopy one can measure the Mott gap [36], and the shell structure of a Mott insulator with different filling numbers has also been observed when the system is deeply in the Mott limit [36, 37]. However, the experiments in the superfluid side and in the quantum critical regime is much less clear. We summarize the major problems as follows:

(1) *How important is the temperature effect in current optical lattice experiments?* As the lattice depth V_0 increases, the BEC temperature drops for two rea-

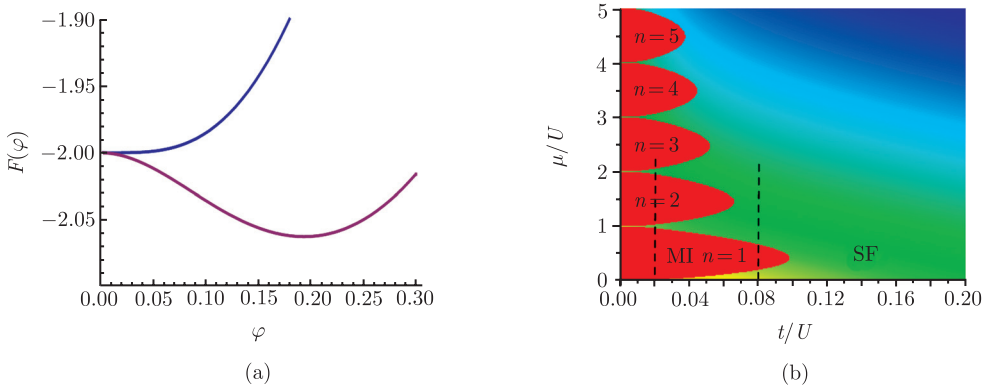

Fig. 10 **(a)** The ground state energy of $\boldsymbol{H}_i$, $F(\varphi)$ in units of U, as a function of φ for small t/U in Mott insulator phase, and for large t/U in superfluid phase, respectively. **(b)** The phase diagram of Boson Hubbard model. The red areas are the Mott insulator phases with different number of bosons per site. The horizontal axes is t/U and the vertical axes is μ/U.

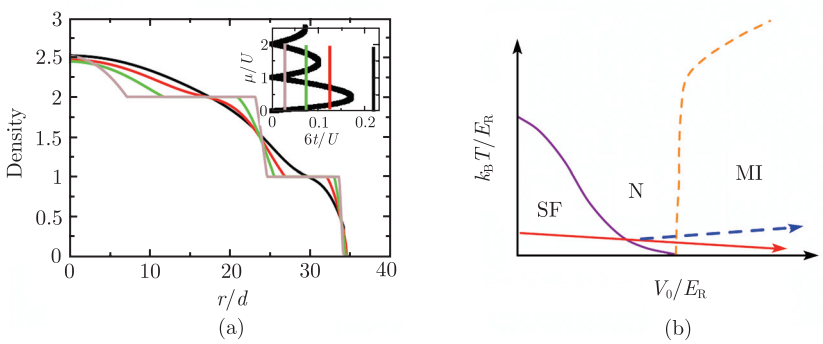

Fig. 11 **(a)** The real space density profile for different values of t/U. The inset indicates the corresponding local chemical potential trajectory in the phase diagram. This figure was published in Ref. [39]. **(b)** A schematic of the finite temperature phase diagram in terms of temperature $k_{\rm B}T$ and lattice depth V_0. The superfluid transition temperature drops exponentially fast with the increase of V_0. The red solid and blue dashed arrows indicate two possible physical trajectories in experiments, and the blue dashed one is more possible.

sons. One is due to the approach of the quantum critical point, and the second is because the hopping amplitude decreases very fast with the increase of V_0. Actually, the second effect is more dramatic which makes the BEC temperature drop exponentially, as schematically shown in Fig. 11(b). In fact, for ^{87}Rb atoms in optical lattices, even without considering the quantum critical effect, the BEC temperature for the gas already drops to nano-Kelvin when $V_0 \sim 10E_{\rm R}$ [38], which is much lower than the initial temperature of the gas before ramping up lattices. Hence, it is conceivable that the superfluid undergoes a thermal phase transition into normal gas way before entering the quantum critical regime, such as the physical trajectory indicated in Fig. 11(b). A recent analysis of the visibility of the measured momentum distribution provides strong evidence that it is the case [39].

(2) *How can we measure temperature in a lattice environment?* In the conventional condensed matter systems, the determination of temperature relies on the thermal reservoir, for instance, we usually use lattice temperature to determine the temperature of an electron gas. Trapped quantum gases is different because it is isolated from any thermal reservoir. As discussed in Section 2.3, in the trapped BEC without lattices, temperature measurement relies on the non-condensed weakly-interacting particles where we know its equation-of-state very well. However, in lattices both thermal excitation and quantum depletion contribute to the non-condensed component, and they are generically mixed and indistinguishable. In the quantum critical regime the equation-of-state is not known for the quantum depletion. So the previous methods of determining temperature all fail, which raises an unsolved problem of how to determine temperature for strongly interacting quantum gases in lattices in a model-independent manner.

(3) *How the system temperature evolves while ramping up the lattices?* In the current way of doing optical lattice experiments, one starts with a condensate or a degenerate Fermi gas without lattices, and then ramps up the lattice potential. Hence, if the ramping process is slow enough to ensure the adiabaticity, the entropy is

conserved, and the temperature may either increase or decrease, depending on the properties of the final quantum state. For instance, when the system approaches and enters the Mott insulator phase where a gap opens in the excitation spectrum, temperature will increase for a fixed entropy [38]. And if some fermions are mixed into the bosons, it will affect the distribution of entropy and strongly affect the temperature of the final state [40]. The distribution of entropy is complicated also because of the inhomogeneity due to the harmonic trap [38]. Understanding how the entropy distributed in the system is very crucial for understanding thermodynamics of trapped quantum gases in lattices.

(4) *How can we cool the quantum gases in the presence of a lattices environment?* Since the kinetic energy scale becomes so small in lattices, one has to cool the system down to below nano-Kelvin in order to reach quantum degeneracy in a lattice environment, which is at least two orders of magnitudes lower than the temperature attainable currently. Besides, since the current ramping scheme usually heats up the system even more, and the current schemes of cooling quantum gases do not work in the presence of a lattice, a brand new scheme is highly desirable.

These issues are important and serious questions in order to make further experimental breakthroughs in this direction, and they are also issues that need more theoretical inputs.

3.2 Repulsive Fermions in lattices

In this section we will first discuss two-component fermions in optical lattices when the interaction is weaker compared to the band gap. When the filling number is smaller than two, it can be described by a single s-band Hubbard model such as

$$\boldsymbol{H} = -t\sum_{ij,\sigma} c^{\dagger}_{i\sigma}c_{j\sigma} + U\sum_{i}\hat{n}_{i\uparrow}\hat{n}_{i\downarrow} - \mu\sum_{i}(\hat{n}_{i\uparrow}+\hat{n}_{i\downarrow}) \quad (25)$$

This model has a very rich phase diagram when one varies the interaction parameter U/t, the filling number (or the chemical potential μ), the lattice geometry and the dimensionality. Despite the huge amount of efforts extending over decades, there are still controversial issues in this model. This model has attracted considerable attention particularly after the 1980s because many people believe that the physics of superconductivity in cuprates can be described by a two-dimensional Hubbard model in the limit of large U/t, and therefore a long-standing theoretical issue arises on whether a two-dimensional Hubbard model can exhibit d-wave superconducting ground state when it is slightly doped away from half-filling. Trapping two-component fermions in optical lattices now offers the promise of simulating the Hubbard model directly, which perhaps can shed new light on many unsolved problems in this model.

Here, instead of discussing the controversial issues, we review the most clean theoretical conclusion about this model, that is, in a half-filled cubic lattice, the system exhibits antiferromagnetic (AF) order at low temperatures. There are two reasons for which we start with AF order. First, in the large U/t limit the AF order is caused by strongly correlated superexchange effect, which is the dominative physics effect in the strongly interacting regime, and secondly, observing this AF order in cold atom experiments is the first step for studying the Hubbard model in this new setup, and it is also the most challenging step at the current stage.

In a half filled cubic lattice, AF order exists for all range of repulsive interactions. For weak interactions, the AF order is caused by mean-field effect which can be described by the standard Hatree-Fock type mean-field theory. The key concept is the nesting of the Fermi surfaces. For instance, as shown in Fig. 12(a), the Fermi surface of a single-band Hubbard model has a perfect nesting at momentum $\{\pi,\pi,\pi\}$, i.e. for any momentum $\boldsymbol{p}$ at the Fermi surface, $\boldsymbol{p}+\{\pi,\pi,\pi\}$ is also a momentum at the Fermi surface. The relation between Fermi surface nesting and AF instability can be understood by performing a particle-hole transformation for one spin species, say,

$$c^{\dagger}_{i,\downarrow} \to (-1)^i c_{i,\downarrow} \quad \text{and} \quad c_{i,\downarrow} \to (-1)^i c^{\dagger}_{i,\downarrow} \quad (26)$$

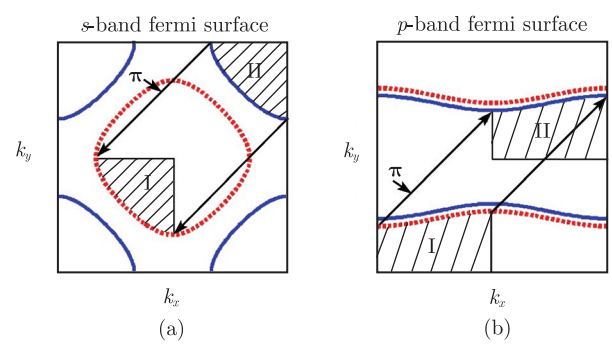

Fig. 12 Schematic of the exact particle-hole symmetry and Fermi surface nesting at half-filling. Red line and blue line are the Fermi surfaces in k_x-k_y plane for $k_z=\pi/3$ and $k_z=-2\pi/3$, respectively. These two Fermi surfaces are separated by the nesting momentum $\vec{\pi}=(\pi,\pi,\pi)$(*the solid black arrow*) for single s-band case **(a)** and for half-filled p-band case **(b)**. Before Eq. (26), the regime-II is filled by holes. The transformation Eq. (26) makes regime-II occupied by $\downarrow$ particles and translates regime-II to regime-I by shifting a vector of $\boldsymbol{\pi}$. $\uparrow$ particles always occupy regime-I. Hence, this shows that in the attractive-U model two-spin components have the same shape of the Fermi surface.

What this transformation does is to first change spin-

down hole packet (shaded area II in Fig. 12) into spin-down particle pocket, and then shift it by a momentum of $\{\pi,\pi,\pi\}$. If the original Fermi surface has perfect nesting at $\{\pi,\pi,\pi\}$, then after this transformation, the new Fermi surface for a spin-down particle is perfectly coincident with that of spin-up particle. Besides, the interaction changes from repulsive to attractive. Hence, the model after the transformation will exhibit BCS instability, which leads to a superconducting order of $\langle c^\dagger_{i,\uparrow}c^\dagger_{i,\downarrow}\rangle \neq 0$, and this superconducting order corresponds to the AF order of $\langle(-1)^i c^\dagger_{i,\uparrow}c_{i,\downarrow}\rangle \neq 0$ upon the particle-hole transformation. That is to say, with the nesting, the AF order can be essentially understood as Fermi surface instability in the exact same way as that in the BCS theory. The Neel temperature for the onset of the AF order, similar to T_c for superconductivity, goes as $e^{-|U|\mathcal{D}(\mathcal{E}_F)}$, where $\mathcal{D}(\mathcal{E}_F)$ is the density of state around the Fermi energy. The presence of the AF order will double the unit cell of the cubic lattice so that the half-filling becomes effectively an integer filling, and the system will open up a charge gap below the Neel temperature when the AF order is sufficiently strong.

In the strongly interacting regime where $U/t \gg 1$, this mean-field theory fails to work. In the absence of hopping, all the sites are singly occupied and each site has an undetermined spin degree of freedom so that the ground state is totally 2^N fold degenerate. This spin degeneracy can be lifted when hopping is included. To the second order perturbation of the hopping term, a Heisenberg model can be derived to describe the low energy spin degrees of freedom [41, 42]

$$\mathcal{H}_H = J_{\rm ex}\sum_{ij}\left(\boldsymbol{S}_i\boldsymbol{S}_j - \frac{n_i n_j}{4}\right) \tag{27}$$

where

$$J_{\rm ex} = \frac{4t^2}{U} \tag{28}$$

and $\boldsymbol{S}_i$ is the on-site spin-1/2 operator defined as

$$\boldsymbol{S}_i = \frac{\hbar}{2}\sum_{ss'} c^\dagger_{i,s}\boldsymbol{\sigma}_{ss'}c_{i,s'} \tag{29}$$

where $\boldsymbol{\sigma}$ are three Pauli matrices. Since $J_{\rm ex}$ is positive, the ground state will be an antiferromagnetic state in a cubic lattice. It happens that this AF state is the same as what we obtained in the weakly interacting regime. However, the driven mechanism is completely different, and the Neel temperature in the strongly interacting regime is $\sim J_{\rm ex}$ which no longer depends on the Fermi surface properties.

Therefore, we have reached the phase diagram for the repulsive Hubbard model as shown in Fig. 13(a). Regime-I is an antiferromagnetic insulator, regime-II is a paramagnetic Mott insulator with no spin order, and regime-III is a paramagnetic Fermi liquid. Note that with the particle-hole transformation mentioned above, the phase diagram for the attractive Hubbard model has the same topology. In the attractive Hubbard model, a BCS superfluid is the ground state in the weakly interacting regime. In the strongly interacting regime, Cooper pairs all become on-site pairs. $J_{\rm ex}$ can be viewed as the hopping amplitude of Cooper pairs, and the Neel temperature can be viewed as the BEC temperature of these on-site pairs. The regimes I-III are the BCS-BEC superfluid, the pseudo-gap phase and the normal Fermi liquid, respectively. The correspondence between the repulsive and the attractive Hubbard model are further summarized in the Table 1. This mapping also establishes the relation between the spin imbalanced Fermi gas with at-

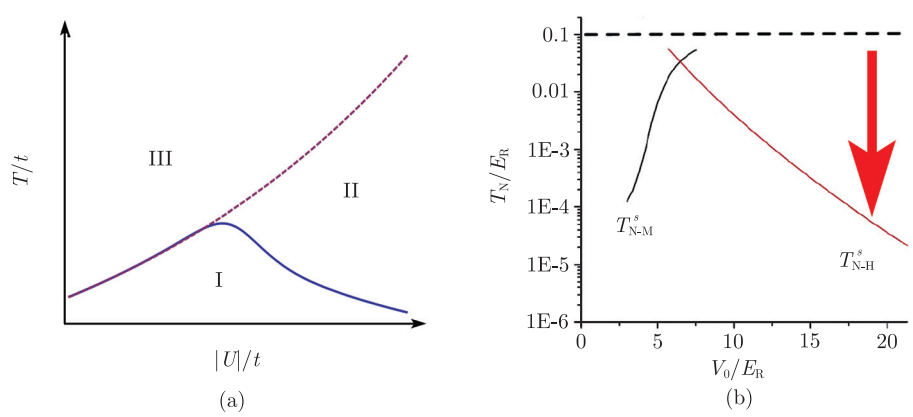

Fig. 13 **(a)** The phase diagram for half-filled repulsive-U Hubbard model and also for equal spin population attractive-U Hubbard model. **(b)** The Neel temperature for fermions in optical lattices with a half-filled s-band. The two solid lines are weakly interacting regime mean-field Neel temperature $T^s_{\text{N-M}}$ and strongly interacting regime Heisenberg model Neel temperature $T^s_{\text{N-H}}$. The dashed line indicates current temperature regime and the red arrows indicate the long way to reach super-exchange physics in this system. The energy units is taken as $E_{\rm R}$, which corresponds to 0.21 μK.

Table 1 The relation between repulsive interaction and attractive interaction Hubbard model under the particle-hole mapping of Eq. (26).

Kinetic term $-t\sum_{ij\sigma} c^\dagger_{i\sigma}c_{j\sigma}$	Kinetic term $-t\sum_{ij\sigma} c^\dagger_{i\sigma}c_{j\sigma}$
Interaction term $U\sum_i \left(n_{i\uparrow}-\frac{1}{2}\right)\left(n_{i\downarrow}-\frac{1}{2}\right)$	Interaction term $-U\sum_i \left(n_{i\uparrow}-\frac{1}{2}\right)\left(n_{i\downarrow}-\frac{1}{2}\right)$
Chemical potential $\mu\sum_i c^\dagger_{i\uparrow}c_{i\uparrow}+c^\dagger_{i\downarrow}c_{i\downarrow}$	Zeeman field $\mu\sum_i c^\dagger_{i\uparrow}c_{i\uparrow}-c^\dagger_{i\downarrow}c_{i\downarrow}$
Zeeman field $h\sum_i c^\dagger_{i\uparrow}c_{i\uparrow}-c^\dagger_{i\downarrow}c_{i\downarrow}$	Chemical potential $\mu\sum_i c^\dagger_{i\uparrow}c_{i\uparrow}+c^\dagger_{i\downarrow}c_{i\downarrow}$
Half filling $N_\uparrow+N_\downarrow=N$	Equal population $N_\uparrow=N_\downarrow$
Doping half-filling $N_\uparrow+N_\downarrow=N+\delta$	Spin imbalance $N_\uparrow=N_\downarrow+\delta$
Antiferromagnetic state at $\boldsymbol{\pi}$ $\langle S^+\rangle=(-1)^i\lvert S\rvert\neq 0$	Uniform BCS state $\Delta\neq 0$
Charge insulator but spin liquid	Pairing without superfluidity

tractive interaction and the repulsive interacting Fermi gases doped away from half-filling.

To explicitly reveal the major difficulty in experiments, we calculate the Néel temperature as a function of lattice depth given by both the mean field formula $T_{\text{N-M}}$ and the Heisenberg model formula $T_{\text{N-H}}$ [43], with the parameters t and U obtained from solving a single particle Schrödinger equation in optical lattice potential, and the result is displayed in Fig. 13(b). For small V_0, $T_{\text{N-M}}\ll T_{\text{N-H}}$, the AF order is caused by mean-field effect, while for large V_0 where $T_{\text{N-H}}\ll T_{\text{N-M}}$, the AF order is driven by super-exchange processes. The regime where $T_{\text{N-M}}$ and $T_{\text{N-H}}$ cross is the crossover regime from weak to strong interaction, where both two methods will fail, and more advanced numerical techniques like dynamic mean-field theory and quantum Monte Carlo is required in order to give accurate Néel temperature [44−46]. However, the key point is that the $T_{\text{N-H}}$ is already of the order of 0.1 nK when the lattice height barely enters the strongly correlated regime, and it decreases below 10^{-2}nK rapidly as V_0 increases. While the lowest temperature attainable nowadays is about 10 nK as indicated by the dashing line in Fig. 13(b). Again, this requires great idea to further cool the system in the presence of lattices for two to three orders of magnitudes in order to reveal superexchange effects.

The underlying reason for this difficulty is due to the rapid decrease of hopping amplitude t with the increase of lattice depth, thus, an alternative way out is to investigate higher band physics where the hopping amplitude is relatively larger for the same lattice depth. For instance, when each lattice site is filled by five fermions, two of them fill the s-band, and the other three will half fill the three-fold degenerate p-band.

The p-band Hubbard model is now much more complicated than the single s-band Hubbard model. Very remarkably, it can be shown that they share very similar physics [47]. One can show that in the strongly interacting regime, at each isolated site the ground state of three fermions in p-orbitals are four-fold degenerate spin-3/2 states due to the Hund's rule coupling. The coupling between two neighboring spins is caused by virtual hopping of fermions, which gives rise to an isotropic spin-3/2 Heisenberg model:

$$\boldsymbol{H}_J = J_{\text{ex}}\sum_{\langle ij\rangle}\left(\boldsymbol{S}_i\boldsymbol{S}_j-\frac{1}{4}n_in_j\right) \tag{30}$$

and $\boldsymbol{S}_i$ is an on-site spin-3/2 operator defined as

$$\boldsymbol{S}_i=\frac{1}{2}\sum_{p_\alpha}\sum_{ss'}c^\dagger_{i,p_\alpha,s}\boldsymbol{\sigma}_{ss'}c_{i,p_\alpha,s'} \tag{31}$$

where $c^\dagger_{i,p_\alpha,s}$ creates a fermion in the p_α orbital of site-i with spin s. J_{ex} is positive that means the ground state possesses spin-3/2 antiferromagnetic order $\langle S_i^+\rangle=(-1)^i|\langle S_i^+\rangle|\neq 0$. In the weakly interacting regime, the Fermi surface of a half-filled p-band also exhibits a perfect nesting symmetry, with the nesting momentum $\boldsymbol{\pi}=(\pi,\pi,\pi)$, as shown in Fig. 12(b). Mean-field analysis shows that this nesting will induce the AF order $\Delta=\langle\sum_{\boldsymbol{k},p_\alpha}c^\dagger_{\boldsymbol{k},p_\alpha\uparrow}c_{\boldsymbol{k}+\boldsymbol{\pi},p_\alpha,\downarrow}\rangle\neq 0$ at low-temperature, and the order parameter also coincides with the $S=3/2$ spin order in the strongly interacting regime. However, the key point is that the Néel temperature for p-band AF order, as shown in Fig. 14, is significantly higher. It remains at the order of nK in deep lattice regime which is a great advantage to access the strongly correlated regime experimentally.

3.3 Lattice Fermi gases across a Feshbach resonance

Across a Feshbach resonance, since the interaction is so strong, more than one band will be involved even in the deep lattice limit where the band gap is very large. This

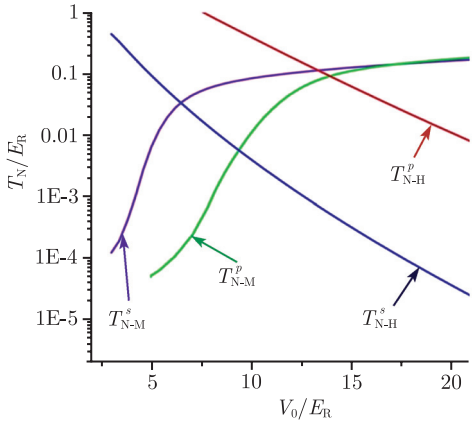

Fig. 14 Néel temperature T_N as a function of optical lattice depth V_0. Four curves are p-band T_N from Heisenberg model $T^p_{N\text{-}H}$, from mean-field theory $T^p_{N\text{-}M}$; s-band T_N from Heisenberg model $T^s_{N\text{-}H}$, from mean-field theory $T^s_{N\text{-}M}$, respectively. For parameters, we use ^{40}K in optical lattices as an example [48]. The lattice spacing $\lambda = 1064$ nm, $K = \pi/\lambda$ and $a_s = 15$ nm. The energy units is taken as E_R, which corresponds to 0.21 μK. This figure was fist published in Ref. [47].

can be demonstrated by solving a two-particle problem in a single harmonic trap, which has been done in Ref. [49] using a single-channel model and later in Ref. [50] with a two-channel model. The solution shows that at least three energy levels, which correspond to three bands when different sites are coupled, will be significantly populated across a Feshbach resonance. Meanwhile, an experiment has also demonstrated the population of higher bands when swapping the magnetic field through a Feshbach resonance [48]. Involving multi-band is also a requirement of recovering the physics at the molecular side properly, since it must be a superposition of multi-band in order that the size of a molecule can be smaller than that of the lowest wannier wave function.

Since a Fermi gas can be changed continuously from a BCS to a BEC superfluid as a function of scattering length, the question is how the entire BCS-BEC family is affected by a lattice potential. The first experiment on this issue was reported from MIT [51] where it was found that at resonance the interference pattern is smeared out when the lattice is increased to about $(3-4)E_R$ deep.

On the molecular side, when the molecule binding energy is much larger than any other energy scales in the problem, the system can be effectively described by a Boson-Hubbard model of molecules, and as discussed in Section 3.1, the transition will be from a boson superfluid to a Mott insulator with integer bosons, i.e. even number of fermions, per lattice site [32]. Whereas on the fermion side, increasing the lattice height V_0 will lead to a transition from a BCS superfluid to a fermion band insulator. This transition is driven by the competition between interaction energy gain by promoting fermions from filled bands to various conduction bands to form Cooper pairs and the kinetic energy cost in overcoming the band gap. It is interesting to note that in most solid state material the band gap (~ 1 eV) is several orders of magnitude larger than the typical pairing energy ($\sim 0.1-10$ meV), and it is impossible for pairing energy to compete with band gap. While the situation is very different in the strongly interacting Fermi gases, the pairing energy is comparable to the Fermi energy, and the band gap is highly tunable. This offers a unique opportunity to study the competition between pairing and lattice effects. A mean field theory description of this transition is developed in Ref. [52].

While it is the same transition for two sides, the properties of the superfluid and insulating phases are continuously changed across the resonance. Since the effects of pair fluctuation are weak in the BCS regime but become increasingly strong in the BEC regime, mean field theory is only accurate on the BCS side of the resonance, less accurate near resonance and becomes very poor on the BEC side. The situation is identical to calculating T_c for the BEC-BCS crossover, where fluctuation corrections grow rapidly on the BEC side [23]. A theory incorporating this fluctuation, i.e. a generalization of the work of Noziéres and Schmitt-Rink [23] to zero temperature with lattices, is highly desirable, which is very essential for obtaining the critical lattice depth at resonance regime correctly and for comparing with experiments properly.

Though there is a lack of a precise understanding at resonance, we can still make a schematic of the global phase diagram in the space of chemical potential μ, lattice height V_0, and interaction parameter $-1/(Ka_s)$ with the help of our knowledge at two sides, as shown in Fig. 15. In the case of two fermions per site, as V_0 increases, the ground state on the BCS side will be a band insulator, whereas it will be a Mott insulator with one boson per site on the BEC side. Because a band insulator can be written as a Fock state with two fermions in the same Wannier state on each site, a band insulator can also evolve continuously into a Mott insulator by simply changing the wavefunction of a fermion pair on each site, and it is also a crossover from a fermion band insulator to a molecular Mott insulator. However, note that while filling the lowest s band requires two fermions per site, filling an additional p band requires totally eight fermions per site, due to the degeneracy of p-band. The Mott insulators on the BEC side, however, can have any integer number of bosons, or any even integer number of fermions per site. Hence, to go from the BEC side to the BCS side, only Mott phases with 1 and 4 bosons can crossover to a band insulator. Mott phases with 2 and 3

bosons (or 4 and 6 fermions) per site must disappear as it approaches the fermion side. It is also an intriguing unsolved issue how the transition from a molecular Mott insulator to a metallic Fermi liquid takes place.

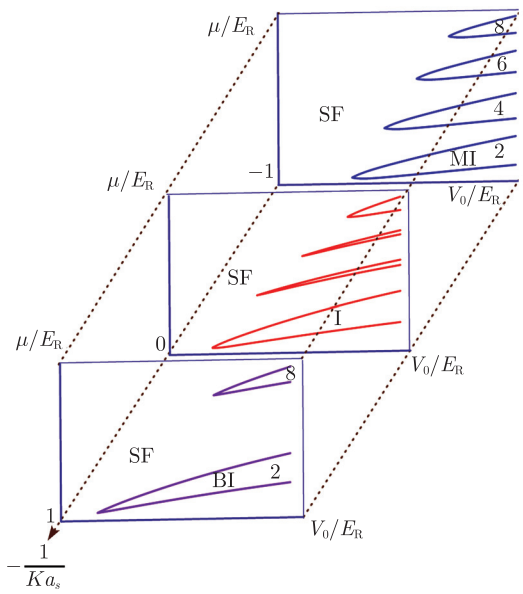

Fig. 15 Schematic of how the μ-V_0 phase diagram evolves across a Feshbach resonance, from the molecule side (*up one*) to the resonance regime (*middle one*) to the fermion side (*bottom one*). This figure was fist published in Ref. [52].

4 Fast rotating quantum gases

When a trapped quantum gas is rotated along the z-direction with a frequency Ω, its single particle Hamiltonian becomes

$$H_0 = \frac{\hbar^2}{2m}\nabla^2 - \Omega L_z + \frac{1}{2}m\omega^2 r^2 + \frac{1}{2}\omega_z^2 z^2 \tag{32}$$

which can be rewritten as

$$H_0 = \frac{1}{2m}\left(\hat{p} - m\Omega\hat{z}\times\boldsymbol{r}\right)^2 + \frac{1}{2}m(\omega^2-\Omega^2)r^2 + \frac{1}{2}\omega_z^2 z^2 \tag{33}$$

We note that the first term in Eq. (33) is exactly the same as the Hamiltonian of an electron moving in a magnetic field along z-direction, the single particle spectrum of which are Landau levels with a level spacing $\hbar\Omega$. The last two terms in Eq. (33) are residual trapping potential which can be treated by the local density approximation as usual. An interacting electron gas in Landau levels has been previously investigated in the quantum well systems, where both integer and fractional quantum Hall effects have been discovered and studied extensively. In this section, we will review some recent progresses in studying both the ultracold boson and fermion gases in the Landau level regime.

4.1 Bosons in lowest Landau level

Rotation will create vortices in a Bose-Einstein condensate. Usually, the average distance between two vortices d is given by the "magnetic length" $\sqrt{\hbar/(m\Omega)}$, while the size of a vortex core ξ is given by the healing length of the condensate $\hbar/\sqrt{2mgn}$, where g is the strength of the local interaction and n is the density of the condensate. For a dense quantum liquid like ^{4}He superfluid where n is very high, or for a slowly rotating condensate where Ω is small, $\xi \ll d$, therefore vortices can be viewed as point defects in a superfluid.

Because n is small in a condensate of dilute gas, it is experimentally accessible that ξ can be comparable or even larger than d. In other words, the vortex core will begin to overlap. We note that $\xi > d$ is equivalent to $gn < \hbar\Omega$, that is to say, the interaction is not able to excite particles into higher Landau levels. So the bosons will almost all condense into the lowest Landau level (L.L.L.). We can therefore project the condensate wave function into the L.L.L. as $\Psi_{\text{L.L.L.}}(r) = \mathcal{P}_{\text{L.L.L.}}\Psi(r)$. In the L.L.L., the wave function is an analytical function of the complex coordinate $w = x + \mathrm{i}y$ apart from an overall Gaussian envelope, i.e. $\Psi_{\text{L.L.L.}} = \prod_i (w - w_i)$, where w_i's denote the locations of vortices. Very importantly, in the L.L.L. regime, $H_0\Psi_{\text{L.L.L}} = \hbar\Omega\Psi_{\text{L.L.L.}}$ which is independent of the positions of vortices. This property of the L.L.L. condensate is its major distinction comparing to a conventional condensate. In a conventional condensate, the kinetic energy logarithmically depends on the distance between two vortices, and therefore the vortices interact with each other logarithmically, which determines the vortex lattice to be a close-packed triangular lattice, as well as vortex dynamics. However, in the L.L.L. condensate, since the kinetic energy is completely quenched, the positions of vortices and the structure of vortex lattices are entirely determined by the interactions between atoms. Nevertheless, it has been shown in Ref. [53] that for a single component condensate with the short range repulsion, the vortex lattice is still a triangular one. Later on the effect of a harmonic trap on the condensate in L.L.L. regime has also been studied [54]. Experiments have also reached the L.L.L. regime [55, 56], and more details of rotating condensate are summarized in a recent review article of Ref. [57].

Here we will give two examples that the interaction between atoms can actually significantly change the vortex lattice structure. The first one is a rotating two-component condensate first proposed by Ref. [58]. For

a weak repulsive interaction between components, two sets of triangular lattices in different components will be staggered so that the vortex core area of one component can fit the high density area of the other component. By maintaining an increase in the repulsion between components, these two sets of lattices will undergo a first order transition from triangular type to square type, and then continuously deformed into rectangular type, in order to further avoid inter-component repulsion. This transition has been observed in experiments [59].

The second example is a rotating dipolar condensate first proposed by Refs. [63] and [64]. We consider both the magnetic dipolar interaction and the short-range s-wave contact interaction between atoms, where the interaction is of the form

$$V = \frac{4\pi\hbar^2 a_s}{m}\delta(\boldsymbol{r}_1 - \boldsymbol{r}_2) + \frac{\mu_0\mu^2}{4\pi}\frac{1}{|\boldsymbol{r}_1 - \boldsymbol{r}_2|^3} \tag{34}$$

The condensate of chromium atoms is such a system [60]. The magnetic dipole moment is six times larger than that of alkali atoms, so its magnetic dipolar interaction is 36 times larger. Also, it has been shown experimentally that its s-wave scattering length can be tuned by Feshbach resonances [61, 62]. Due to the dipolar repulsion, the condensate will not collapse when the s-wave interaction becomes slightly attractive. By using the L.L.L wave function as a trial wave function to minimize the interaction energy, one can show that, when a_s exceeds a certain critical negative value, the vortex lattice will first become a square lattice as the short range attraction increases, and then become more and more rectangular. It eventually forms a structure like arrays of one dimensional stripes, where the density strongly modulates along the direction perpendicular to the stripe, since this arrangement can efficiently benefit the short-range attraction. Finally, the condensate collapses when the s-wave attraction is so strong that it overcomes the dipolar repulsion. The phase diagram is shown in Fig. 16.

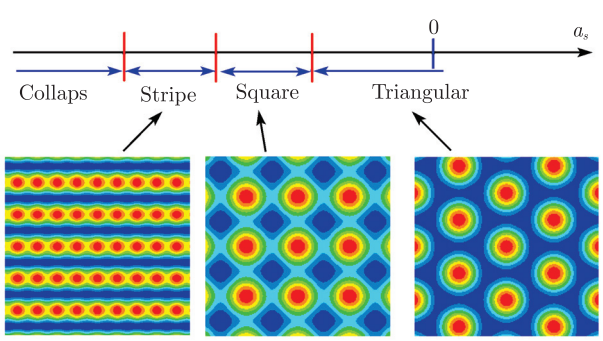

Fig. 16 A sequence of structure transitions of vortex lattices, form the triangular lattice to the square lattice and eventually to the vortex stripe phase, in a fast rotating dipolar condensate.

4.2 Fast rotating Fermi gases

Even for non-interacting fermions, it is very interesting in the fast rotating regime since the integer quantum Hall effect will take place. Inside a trap, the Hall insulator will manifest itself in the density profile as a sequence of plateaus [65], which is due to the same reason as the wedding cake structure discussed in Section 3.1. In addition to rotation, if one imposes an optical lattice, it will become more interesting since the single particle spectrum will behave as Hofstadter butterfly [66], which is topological in nature [67]. The manifestation of the Hofstadter insulator can also be revealed in the density profile, and from the density profile one can also measure the Hall conductance without doing transport experiments [68]. In particular, we emphasize the fact that the effective "magnetic field" created by rotation can be as large as hundreds and thousands Tesla, which is not attainable for any real magnetic field in a laboratory [68].

In this section, we will mainly focus on how the BEC-BCS family responds to the external rotation across a resonance. An experiment has succeeded in creating vortex lattices in the fermion superfluid from the BCS to the BEC regime [69], and this is analogous to the vortex lattices in the type-II superconductors in a magnetic field. It is well known that a superconductor will turn into a normal metal when the magnetic field exceeds a certain critical value known as H_{c2}. Similarly, one expects a fermion pair superfluid will also become normal when it is above some critical rotational frequency Ω_{c2}.

Here we will first introduce the two-channel model for Feshbach resonance in a rotating frame

$$\begin{aligned}\mathcal{H} = &\sum_{\nu\sigma}\xi_\nu f^\dagger_{\nu\sigma} f_{\nu\sigma} + \Xi_0 b^\dagger b \\ &+\alpha\sum_{\nu\nu'}\left(Q^*_{\nu\nu'} b^\dagger f_{\nu\uparrow} f_{\nu'\downarrow} + \text{h.c.}\right)\end{aligned} \tag{35}$$

where $f^\dagger_{\nu\sigma}$ is the creation operator for an open channel fermion with Landau level quantum number ν, spin σ, and energy ξ_ν. $b^\dagger$ creates a close channel molecule, which is restricted in the L.L.L.. It is important to note that restricting the condensate to the L.L.L. imposes no restrictions on the quantum numbers of the fermions. Two fermions in different Landau levels can convert into a molecule in the L.L.L., with the coupling α and an overlap integral $Q_{\nu\nu'} = \int \mathrm{d}\boldsymbol{r}\mathrm{d}\boldsymbol{R}\phi^*_\nu(\boldsymbol{R}+\boldsymbol{r}/2)\phi^*_{\nu'}(\boldsymbol{R}-\boldsymbol{r}/2)D(\boldsymbol{R},\boldsymbol{r})$, where $\boldsymbol{R}$ and $\boldsymbol{r}$ are the center-of-mass and relative coordinate of the fermion pair, and $D(\boldsymbol{R},\boldsymbol{r})$ is the wavefunction of the tightly bound close-channel molecule, which can be taken as $\Phi(\boldsymbol{R})\delta(\boldsymbol{r})$. ϕ_ν is the wave function of the state with quantum number ν, and $\Phi(\boldsymbol{R})$ is a vortex lattice wave function in the

L.L.L.. Here, $\bar{\gamma}$ is the unrenormalized molecular binding energy. To remove the divergency, $\bar{\gamma}$ must be renormalized as $\gamma = \bar{\gamma} - \alpha^2 m/(4\pi\sqrt{2}a\hbar^2)\sum_N 1/\sqrt{N+1}$, where a is the "magnetic length", and the renormalized parameters (γ, α) are related to physical parameters (a_s, r_0) as

$$-\frac{\gamma}{\alpha^2} = \frac{m}{a_s\hbar^2\pi\sqrt{2}}; \quad \frac{1}{\alpha^2} = -\frac{r_0 m^2}{2\pi\sqrt{2}\hbar^4} \tag{36}$$

Within the mean-field theory, we replace $\alpha\langle \boldsymbol{b}\rangle = \Delta$, and the free energy can be expanded in powers of Δ as $\mathcal{F} = \mathcal{F}_0 + \chi|\Delta|^2 + o(|\Delta|^4)$. $\chi < 0 (> 0)$ means that the system is in the superfluid (normal) state. In this way, one can determine the critical rotational frequency Ω_c as a function of a_s, which is shown in Fig. 17. As one approaches the resonance from the BCS side, Ω_c increases and has a sequence of steps. This reflects the periodicity of the density of state in the Landau level spectrum, which is an effect analogous to the integer quantum Hall effect. Since whenever the chemical potential marches an eigenenergy of a Landau level, the large density of state near the Fermi surface due to the Landau level degeneracy will give rise to a strong Cooper instability, which protects the superfluid from being destroyed [70]. This mean-field calculation also shows that the critical rotation only exits at the BCS side, and the superfluidity is robust against pair breaking effect caused by rotation at resonance and in the BEC side [70, 71].

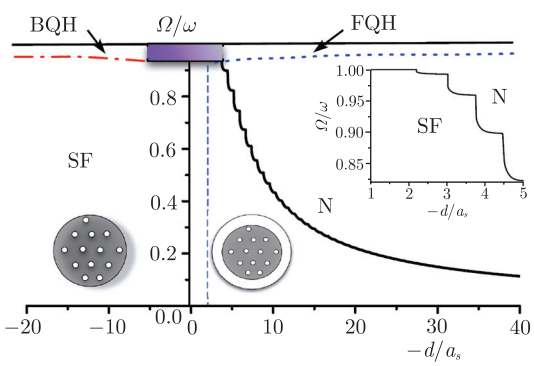

Fig. 17 Phase diagram of a rotating Fermi gas across a Feshbach resonance. In the side $a_s > 0$ "SF" means superfluid with vortices, and in the side $a_s < 0$, below the critical frequency line the system is a coexistence of superfluid with vortices at the center of the trap, and normal state at the outside region. "N" denotes that the whole cloud becomes normal. "FQH" and "BQH" denote fermionic and bosonic quantum Hall states, respectively. The transition regime between two quantum Hall states is indicated by the shaded area, which is not yet quite clear. The inset shows the mean-field critical frequency in the fast rotating regime. A similar figure was first published in Ref. [70].

However, when the quantum fluctuation beyond mean-field is taken into account, even a boson superfluid will be replaced by a bosonic quantum Hall state, when the number of vortices becomes comparable to the number of bosons in the ultra-fast rotation limit [72]. On the other hand, a normal Fermi gas will become a fermionic quantum Hall insulator as the rotation frequency further increases. Therefore, at two different sides of the resonance, one gets two different types of quantum Hall states, the transition between different quantum Hall states is an unsolved problem [73], and the details of the transition will also depend on the filling number.

5 Future prospects

Our current knowledge of quantum many-body physics are all built on the research of solid state materials and quantum liquids. Nowadays, thanks to the advanced technique of trapping, cooling and manipulating atoms and molecules, many laboratories all over the world are performing extensive experimental studies of a host of new quantum many-body models in the dilute quantum gases. In particular, we are now able to control the interactions to be very strong by various means. There is no doubt that this investment will reveal more new physical phenomena and concepts in the near future. However, it is hard to predict which will be the next big discovery in this field, due to the diversity of the research directions. Nevertheless, it is worthwhile to pay sufficient attention to the following directions, since there must be a lot of developments along these in the future: (1) strongly interacting fermions in optical lattices; (2) molecular quantum gases; (3) low-dimensional quantum gases; (4) multi-component mixture, boson-fermion mixture and quantum gases with internal degrees of freedoms and (5) dynamics, non-equilibrium and quantum kinetics in quantum gases.

Acknowledgements This review paper is a result of many fruitful collaborations and discussions with Lee Chang, Zuo-zi Chen, Roberto Diener, Rong Lü, Mehmet Oktel, Rifat Umucal l ar, Kai Wu, Kun Yang, Fei Zhou, Jian Zhang and Qi Zhou during the last few years. In particular, I would like to thank Jason Ho for his helpful guidance, and the collaboration with him is a very happy experience for me, through which I learned a lot. I would also like to sincerely thank Chen-Ning Yang, Hwa-Tung Nieh, Zheng-Yu Weng, Zhan Xu and Nian-le Wu for their encouragement and support throughout all these years.

References

1. F. Dalfovo, S. Giorgini, L. P. Pitaevskii, and S. Stringari, Rev. Mod. Phys., 1999, 71: 463
2. A. J. Leggett, Rev. Mod. Phys., 2001, 73: 307
3. S. Giorgini, L. P. Pitaevskii, and S. Stringari, Rev. Mod.

Phys., 2008, 80: 1215
4. W. Ketterle and M. W. Zwierlein, arXiv: 0801.2500, in: Proceedings of the International School of Physics "Enrico Fermi", Course CLXIV, Varenna, 20−30 June 2006, edited by M. Inguscio, W. Ketterle, and C. Salomon
5. R. Grimm, arXiv: cond-mat/0703091, in: Proceedings of the International School of Physics "Enrico Fermi", Course CLXIV, Varenna, 20−30 June 2006, edited by M. Inguscio, W. Ketterle, and C. Salomon
6. M. Greiner, C. A. Regal, and D. S. Jin, arXiv: cond-mat/0502539
7. See also Section 5.3 of the book " Bose-Einstein Condensate in Dilute Gases", edited by C. J. Pethick and H. Smith, published by Cambridge University Press, where they use $1/r^6$ model potential to demonstrate the scattering
8. R. Diener and T. L. Ho, arXiv: cond-mat/0705174
9. K. Huang and C. N. Yang, Phys. Rev., 1957, 105: 767
10. T. D. Lee, K. Huang, and C. N. Yang, Phys. Rev., 1957, 106: 1135
11. T. D. Lee and C. N. Yang, Phys. Rev., 1957, 105: 1119
12. D. T. Son, Phys. Rev. Lett., 2007, 98: 020604
13. T. L. Ho, Phys. Rev. Lett., 2004, 92: 090402
14. J. Carlson, S. Y. Chang, V. R. Pandharipande, and K. E. Schmidt, Phys. Rev. Lett., 2003, 91: 050401
15. G. E. Astrakharchik, J. Boronat, J. Casulleras, and S. Giorgini, Phys. Rev. Lett., 2004, 93: 200404
16. J. T. Stewart, J. P. Gaebler, C. A. Regal, and D. S. Jin, Phys. Rev. Lett., 2006, 97: 220406
17. G. B. Partridge, W. H. Li, R. I. Kamar, Y. A. Liao, and R. G. Hulet, Science, 2006, 311: 503
18. J. E. Thomas, J. Kinast, and A. Turlapov, Phys. Rev. Lett., 2005, 95: 120402
19. L. Luo, B. Clancy, J. Joseph, J. Kinast, and J. E. Thomas, Phys. Rev. Lett., 2007, 98: 080402
20. D. S. Petrov, C. Salomon, and G. V. Shlyapnikov, Phys. Rev. Lett., 2004, 93: 090404
21. A. J. Leggett, in: Modern Trends in the Theory of Condensed Matter, edited by A. Pekalski and R. Przystawa, Berlin: Springer-Verlag, 1980
22. M. Randeria, in: Bose-Einstein Condensation, edited by A. Griffin, D. W. Snoke, and S. Stringari, Cambridge: Cambridge University Press, 1995
23. P. Noziéres and S. Schmitt-Rink, J. Low. Temp. Phys., 1985, 59: 195
24. M. W. Zwierlein, A. Schirotzek, C. H. Schunck, and W. Ketterle, Science, 2006, 311: 492
25. C. H. Schunck, Y. Shin, A. Schirotzek, M. W. Zwierlein, and W. Ketterle, Science, 2007, 316: 867
26. D. E. Sheehy and L. Radzihovsky, Annals of Physics, 2007, 322: 1790, and references therein
27. E. Wille, F. M. Spiegelhalder, G. Kerner, D. Naik, A. Trenkwalder, G. Hendl, F. Schreck, R. Grimm, T. G. Tiecke, J. T. Walraven, S. J. Kokkelmans, E. Tiesinga, and P. S. Julienne, Phys. Rev. Lett., 2008, 100: 053201
28. M. Bartenstein, A. Altmeyer, S. Riedl, R. Geursen, S. Jochim, C. Chin, J. Hecker Denschlag, R. Grimm, A. Simoni, E. Tiesinga, C. J. Williams, and P. S. Julienne, Phys. Rev. Lett., 2005, 94: 103201
29. A. G. K. Modawi and A. J. Leggett, J. Low. Temp. Phys., 1997, 109: 625
30. H. Zhai, Phy. Rev. A, 2007, 75: 031603
31. T. B. Ottenstein, T. Lompe, M. Kohnen, A. N. Wenz, and S. Jochim, arXiv: cond-mat/0806.0587
32. M. P. A. Fisher, P. B, Weichman, G. Grinstein, and D. S. Fisher, Phys. Rev. B, 1989, 40: 546
33. K. Sheshadri, H. R. Krishnamurthy, R. Pandit, and T. V. Ramakrishnan, Europhys. Lett., 1993, 22: 257
34. M. Greiner, O. Mandel, T. Esslinger, T. W. Hänsch, and I. Bloch, Nature, 2002, 415: 39
35. For a review of these works, see: I. Bloch, J. Dalibard, and W. Zwerger, Rev. Mod. Phys., 2008, 80: 885
36. G. K. Campbell, J. Mun, M. Boyd, P. Medley, A. E. Leanhardt, L. G. Marcassa, D. E. Pritchard, and W. Ketterle, Science, 2006, 313: 649
37. S. Fölling, A. Widera, T. Müller, F. Gerbier, and I. Bloch, Phys. Rev. Lett., 2006, 97: 060403
38. T. L. Ho and Q. Zhou, Phys. Rev. Lett., 2007, 99: 120404
39. R. B. Diener, Q. Zhou, H. Zhai, and T. L. Ho, Phys. Rev. Lett., 2007, 98: 180404
40. M. Cramer, S. Ospelkaus, C. Ospelkaus, K. Bongs, K. Sengstock, and J. Eisert, Phys. Rev. Lett., 2008, 100: 140409
41. E. Fradkin, Field Theories of Condensed Matter Systems, Addison-Wesley Publishing Company, 1991, Chapter 2
42. A. Auerbach, Interacting Electrons and Quantum Magnetism, New York: Springer-Verlag, 1994, Chapter 3.2 and 4.2
43. A. Georges, arXiv: cond-mat/0702122
44. W. Metzner and D. Vollhardt, Phys. Rev. Lett., 1989, 62: 324.
45. A. Georges, G. Kotliar, W. Krauth, and M. J. Rozenberg, Rev. Mod. Phys., 1996, 68: 13
46. M. Jarrell, Phys. Rev. Lett., 1992, 69: 168
47. W. Kai and H. Zhai, Phys. Rev. B, 2008, 77: 174431
48. M Köhl, H. Moritz, T. Stöferle, K. Günter, and T. Esslinger, Phys. Rev. Lett., 2005, 94: 080403
49. T. Busch, B. Englert, K. Rzaźewski, and M. Wilkens, Foundations of Physics, 1998, 28: 549
50. R. B. Diener and T. L. Ho, Phys. Rev. Lett., 2006, 96: 010402
51. J. K. Chin, D. E. Miller, Y. Liu, C. Stan, W. Setiawan, C. Sanner, K. Xu, and W. Ketterle, Nature, 2006, 961: 443
52. H. Zhai and T. L. Ho, Phys. Rev. Lett., 2007, 99: 100402
53. T. L. Ho, Phys. Rev. Lett., 2001, 87: 060403
54. G. Watanabe, G. Baym, and C. J. Pethick, Phys. Rev. Lett., 2004, 93: 190401
55. V. Schweikhard, I. Coddington, P. Engels, V. P. Mogendorff, and E. A. Cornell, Phys. Rev. Lett., 2004, 92: 040404
56. I. Coddington, P. C. Haljan, P. Engels, V. Schweikhard, S. Tung, and E. A. Cornell, Phys. Rev. A, 2004, 70: 063607
57. A. L. Fetter, arXiv: cond-mat/0801.2952

58. E. J. Mueller and T. L. Ho, Phys. Rev. Lett., 2002, 88: 180403
59. V. Schweikhard, I. Coddington, P. Engels, S. Tung, and E. A. Cornell, Phys. Rev. Lett., 2004, 93: 210403
60. A. Griesmaier, J. Werner, S. Hensler, J. Stuhler, and T. Pfau, Phys. Rev. Lett., 2005, 94: 160401
61. J. Werner, A. Griesmaier, S. Hensler, J. Stuhler, T. Pfau, A. Simoni, and E. Tiesinga, Phys. Rev. Lett., 2005, 94: 183201
62. T. Koch, T. Lahaye, J. Metz, B. FrAhlich, A. Griesmaier, and T. Pfau, Nature Physics, 2008, 4: 218
63. J. Zhang and H. Zhai, Phys. Rev. Lett., 2005, 95: 200403
64. N. R. Cooper, E. H. Rezayi, and S. H. Simon, Phys. Rev. Lett., 2005, 95: 200402
65. T. L. Ho and C. V. Ciobanu, Phys. Rev. Lett., 2000, 85: 4648
66. D. R. Hofstadter, Phys. Rev. B, 1976, 14: 2239
67. D. J. Thouless, M. Kohmoto, M. P. Nightingale, and M. den Nijs, Phys. Rev. Lett., 1982, 49: 405
68. R. O. Umucallar, H. Zhai, and M. Ö. Oktel, Phys. Rev. Lett., 2008, 100: 070402
69. M. W. Zwierlein, J. R. Abo-Shaeer, A. Schirotzek, C. H. Schunck, and W. Ketterle, Nature, 435: 1047
70. H. Zhai and T. L. Ho, Phys. Rev. Lett., 2006, 97: 180414
71. M. Y. Veillette, D. E. Sheehy, L. Radzihovsky, and V. Gurarie, Phys. Rev. Lett., 2006, 97: 250401
72. N. R. Cooper, N. K. Wilkin, and J. M. Gunn, Phys. Rev. Lett., 2001, 87: 120405
73. K. Yang and H. Zhai, Phys. Rev. Lett., 2008, 100: 030404